

# GAMMA RAY BURSTS AND SUPERNOVA SIGNATURES IN SLOWLY ROTATING COLLAPSARS

DIEGO LOPEZ-CAMARA, WILLIAM H. LEE

Instituto de Astronomía, Universidad Nacional Autónoma de México, Apdo. Postal 70-264, Cd. Universitaria, México D.F. 04510,  
(dlopez,wlee)@astroscu.unam.mx

AND

ENRICO RAMIREZ-RUIZ

Department of Astronomy and Astrophysics, UCO/Lick, University of California, Santa Cruz, Santa Cruz, CA, 95060,  
enrico@ucolick.org

*Accepted by ApJ*

## ABSTRACT

We consider accretion onto newborn black holes (BHs) following the collapse of rotating massive stellar cores, at the threshold where a centrifugally supported disk gives way to nearly radial inflow for low angular momentum. For realistic initial conditions taken from pre-supernova (pre-SN) evolution calculations, the densities and temperatures involved require the use of a detailed equation of state and neutrino cooling processes, as well as a qualitative consideration of the effects of general relativity. Through two-dimensional dynamical calculations we show how the energy release is affected by the rotation rate and the strength of angular momentum transport, giving rise to qualitatively different solutions in limits of high and low angular momentum, each being capable of powering a gamma-ray burst (GRB). We explore the likelihood of producing Fe-group elements in the two regimes and suggest that while large and massive centrifugally supported disks are capable of driving strong outflows with a possible SN-like signature, quasi-radial flows lack such a feature and may produce a GRB without such an accompanying feature, as seen in GRB060505.

*Subject headings:* accretion, accretion disks — hydrodynamics — gamma rays: bursts — supernovae

## 1. INTRODUCTION

Gamma-ray bursts (GRBs) have remained as an outstanding problem in astrophysics since their discovery in 1967 (Klebesadel et al. 1973). Major advances in their understanding came through observational breakthroughs following BATSE, which provided an extensive all-sky catalog (Fishman & Meegan 1995) and the identification of counterparts at lower energies at high redshift (Metzger et al. 1997) through Beppo Sax (van Paradijs et al. 2000) and Swift (Gehrels et al. 2007). Isotropic equivalent energies range from  $10^{49}$  erg s<sup>-1</sup> to  $10^{52}$  erg s<sup>-1</sup>, coming from sources at redshifts as high as  $z \simeq 6$  that are randomly distributed over the sky (Meegan et al. 1992). GRBs are commonly divided into short (SGRBs, less than 2 seconds in duration, typically at redshift  $z \simeq 1$  and frequently in host galaxies with low star formation rates (SFRs)) and long (LGRBs, longer than 2 seconds, residing at  $z \simeq 1 - 5$  in star forming galaxies) events. An additional distinction is that those of the short variety tend to have harder spectra, hence the short-hard/long-soft denomination (Dezalay et al. 1996). Recently there appears to be a substantial and, in some respects, puzzling overlap between the two populations, and it has been suggested that a third group or even a new classification is necessary (Gehrels et al. 2006; Gal Yam et al. 2006; Della Valle et al. 2006b; Fynbo et al. 2006).

The energy release, short duration, and variability time scales associated with GRBs favor accretion onto compact objects, or magnetically powered events from such objects, as their ultimate source. Many models have been suggested over the years, a number of which were discarded once the global energy budget was fixed through the resolution of the distance scale to the sources. Among the early proposals still considered are compact binary mergers (Lattimer & Schramm 1974, 1976; Paczyński 1986, 1991; Eichler et al. 1989; Narayan et al. 1992), magnetars (Usov 1992; Thompson 1994; Mészáros & Rees 1997) and the collapse of massive stellar cores (Woosley 1993), see (Mészáros 2002; Piran 2004; Nakar 2007; Lee & Ramirez-Ruiz 2007) for reviews.

In general, accretion onto a central object can proceed and release gravitational binding energy efficiently if the gas can cool or otherwise lose its internal energy e.g., through advection, and thus move down in the potential well (Salpeter 1964; Zel'Dovich 1964). At the usual astrophysical scales, this occurs through photons, and produces phenomena ranging from active galactic nuclei (AGN) to low mass X-ray binaries (LMXBs). If the accretion rate is too high though, the fluid may become so optically thick to the photons that they become trapped and are unable to cool the gas. At even higher accretion rates, a different mechanism enters the picture, namely, neutrino cooling. This regime is termed “hypercritical”, since it is far above the usual Eddington limit for photons, and is relevant, for example, in post-supernova cores and the associated fall back, as was probably the case in SN1987A (Chevalier 1989; Houck & Chevalier 1991). It is this phenomenon that is now thought possible of generically powering GRBs. The question at the forefront of attention has been how to achieve these conditions in an astrophysical setting.

There has been mounting evidence in the past few years linking LGRBs at low redshift with type Ic SNe, with spatial and temporal coincidences for a number of events (Woosley & Bloom 2006; Kaneko et al. 2008). Galama et al. (1998) linked for the first time a LGRB with a SN (GRB980425 with SN1998bw). After 27 days the optical spectrum of

GRB980425 resembled that of a H-deficient type Ic SN. To date there have been at least 6 other LGRB/SN connections: XRF020903 (Soderberg et al. 2005); GRB021211 with SN2002lt (Della Valle et al. 2003); GRB030329 with SN2003dh (whose optical spectrum afterglow was strikingly similar to that of SN1998bw (Stanek et al. 2003)); GRB031203 with SN2003lw (Malesani et al. 2004; Ramirez-Ruiz et al. 2005); GRB050525A with SN2005nc (Della Valle et al. 2006a); and GRB060218 with SN2006aj (Campana et al. 2006). In addition, LGRBs in general are associated with low metallicity star-forming regions in their host galaxies (Prochaska et al. 2004; Gorosabel et al. 2005; Sollerman et al. 2005; Fruchter et al. 2006; Fynbo et al. 2006) suggesting a link to massive stars (Bloom, Kulkarni & Djorgovski 2002; Woosley & Bloom 2006).

The observational association with SNe has given support to the idea that LGRBs are produced in the collapse of massive stellar cores. MacFadyen & Woosley (1999) developed this in great detail in the collapsar scenario, assuming a black hole (BH) is formed at the center and evaluating the potential to produce a GRB. The infalling stellar material that is not ejected in the usual SN forms a massive, dense and hot accretion disk which releases the necessary energy to power the burst. They distinguished between Type I and Type II collapsars: the former entails the direct collapse of the iron core to a BH, while in the latter initially a proto-neutron star lies at the center of the star, and later collapses to a BH once it has accreted a sufficient amount of mass. A GRB may be produced even if there is no BH at the center in a magnetically dominated explosion during the proto-neutron star phase of the collapse (Dessart et al. 2008). Here, we will focus on Type I collapsars. The absence of H lines in the observed GRB/SN spectra implies that the progenitor has somehow lost its envelope, perhaps through interaction with a binary companion and/or strong winds, and is thus essentially a Wolf-Rayet (WR) star (Izzard, Ramirez-Ruiz & Tout 2004; Cantiello et al. 2007).

In the standard version of the collapsar, the GRB/SN link is a quite natural consequence, and observed associations have thus provided a strong motivation in this sense to study it further. Typical LGRBs have  $z \simeq 1 - 4$ , which is too far for a SN counterpart to be detected, and indeed, the cases in which there is such a correspondence all lie at fairly low redshift. Two recent events however, GRB060505 and GRB 060614 (Fynbo et al. 2006; Gehrels et al. 2006; Gal Yam et al. 2006; Della Valle et al. 2006b), have pointed perhaps to a different situation in which the GRB is *not* accompanied by a SN. Their low redshift allowed deep searches which convincingly ruled out the presence of an underlying type Ic stellar explosion of the kind seen in SN1998bw and SN2003dh, and particularly, the host of GRB060505 is a star-forming galaxy, similar to that of typical LGRBs (Fynbo et al. 2006). We explore here how the initial angular momentum distribution in the star, and possibly the vigor of angular momentum transport within the centrifugally supported accretion disk, may furnish a key ingredient to understand this behavior.

An important point is that despite considerable effort (see Woosley & Heger (2006)), the stellar rotation rate in pre-SN cores is not fully determined. It can sensitively depend on evolutionary details, such as mass loss on the main sequence and the stellar magnetic field, which both lead to important spin down in later stages (Spruit 2002; Heger et al. 2005). Binary interactions may also affect the rotation rate through tidal interactions (Detmers et al. 2008). We note that Yoon & Langer (2005), and Woosley & Heger (2006), have identified a channel for massive stars in which mass and angular momentum losses are greatly reduced by complete mixing in the main sequence and the consequent absence of a giant phase.

What we do know is that the specific angular momentum,  $J$ , needed to form a disk around the BH is at least the value of the innermost stable circular orbit  $R_{isco}$  ( $R_{isco} = 3r_g$ , where  $r_g = 2GM_{BH}/c^2$  is the Schwarzschild radius) times the velocity of the particles (which are very close to the speed of light). So, a first estimate for the critical  $J$  would be  $J_{crit} = R_{isco}c = 3r_gc = 6GM/c \sim 10^{16} \text{ cm}^2 \text{ s}^{-1}$  for a one solar mass BH (the true critical value is  $J_{crit} \simeq 2r_gc$ , see Section 3.1). Most studies of collapsars and neutrino-dominated accretion flows (MacFadyen & Woosley 1999; Popham, Woosley & Fryer 1999; Heger et al. 2000; Narayan, Piran & Kumar 2001; Proga & Begelman 2003; Proga, MacFadyen, Armitage & Begelman 2003; Lee, Ramirez-Ruiz & Page 2005) have considered angular momentum distributions that are well above this limit and essentially guarantee the formation of a centrifugally supported accretion disk (in stellar core collapse calculations as well as disk evolution studies). In practice, there is also something akin to a maximum value of angular momentum for the collapsar model to work, since for very rapid rotation the accretion disk forms at large radii and the binding energy cannot be effectively dissipated as neutrinos (MacFadyen & Woosley 1999; Lee & Ramirez-Ruiz 2006). Clearly in the limit of slow rotation the accretion disk will form very near the BH, and so general relativity (GR) will play an important role in its evolution.

Our general objective is to explore the morphology, energy release, and observable signatures of hypercritical accretion flows from massive stellar core collapse for a range of angular momentum values covering the transition from centrifugally supported disks to near radial inflow (lying below those usually considered in collapsar calculations) in order to better understand the possible production of LGRBs as well as their putative progenitors. We improve upon previous studies (MacFadyen & Woosley 1999; Proga, MacFadyen, Armitage & Begelman 2003; Lee & Ramirez-Ruiz 2006) in significant ways by considering more detailed thermodynamics in the equation of state, an improved treatment of neutrinos, and through realistic initial conditions taken from evolutionary calculations of Woosley & Heger (2006).

We first describe the input physics and numerical setup in Section 2, followed by our results in Section 3. Prospects for GRB production and the link between SN and GRBs are given in Section 4.

## 2. INPUT PHYSICS

### 2.1. Equation of State and cooling processes

We use a detailed equation of state (Lee, Ramirez-Ruiz & Page 2005) where the total pressure,  $P$ , contains contributions from an ideal gas of  $\alpha$  particles and free nucleons in nuclear statistical equilibrium (NSE),  $P_{\text{gas}}$ , blackbody radiation,  $P_{\text{rad}}$  (the optical depth to photons in the gas is such that they are fully trapped), neutrinos,  $P_\nu$ , and relativistic electron/positron pairs of arbitrary degeneracy,  $P_{e^\pm}$  (Blinnikov, Dunina-Barkovskaya & Nadyozhin 1996). We allow for neutronization and a correspondingly variable electron fraction  $Y_e$  by requiring charge neutrality and equilibrium in weak interactions, depending on whether the fluid is optically thick or thin to its own neutrino emission (Beloborodov 2003; Lee, Ramirez-Ruiz & Page 2005).

The physical conditions in the accretion flow within the collapsing stellar core are such that the temperature and density is  $T \simeq 10^9 - 10^{10}$  K, and  $\rho \simeq 10^8 - 10^{10}$  g cm $^{-3}$  respectively. Thus the reaction rates that will dominate the neutrino emissivities,  $\dot{q}_\nu$ , are  $e^\pm$  capture onto free nucleons ( $\dot{q}_{\text{cap}}$ ) and  $e^\pm$  annihilation ( $\dot{q}_{\text{ann}}$ ), for which we use the tables of Langanke & Martínez-Pinedo (2001) and the fitting functions of Itoh et al. (1996), respectively<sup>1</sup>. Finally, photodisintegration and synthesis of  $\alpha$  particles can also cool or heat the gas, and is correspondingly accounted for (see also Lee, Ramirez-Ruiz & Page (2005)).

If the fluid is optically thin, the total cooling is simply the sum of the emissivities described above. At a finite optical depth, we may split it into scattering and absorption components as  $\tau_\nu = \tau_{\text{scat}} + \tau_{\text{abs}}$ , where the absorption term is due to the inverse reaction of  $e^\pm$  capture onto protons or neutrons,  $\tau_{\text{abs-cap}}$ , and  $\nu\bar{\nu}$  annihilation,  $\tau_{\text{abs-ann}}$  (Di Matteo, Perna & Narayan 2002):

$$\tau_{\text{abs}} = \tau_{\text{abs-cap}} + \tau_{\text{abs-ann}}, \quad (1)$$

with

$$\tau_{\text{abs-cap}} = \frac{2 \dot{q}_{\text{cap}} H}{7 \sigma_{\text{SB}} T^4} \quad (2)$$

$$\tau_{\text{abs-ann}} = \frac{2 \dot{q}_{\text{ann}} H}{7 \sigma_{\text{SB}} T^4}, \quad (3)$$

$H$  being the pressure scale height in the disk and  $\sigma_{\text{SB}}$  the Stefan–Boltzmann constant.

The contribution from scattering off free nucleons is

$$\tau_{\text{scat}} = 13.8 (C_{s,p} Y_p + C_{s,n} Y_n) \frac{\sigma}{m_{\text{u}}} (k_{\text{B}} T / m_e c^2)^2 \rho H, \quad (4)$$

where  $Y_n$  and  $Y_p$  are the neutron and proton fractions,  $C_{s,p} = (1 + 5\alpha^2)/24$ ,  $C_{s,n} = [4(C_v - 1)^2 + 5\alpha^2]/24$ ,  $C_v = 0.5 + 2 \sin^2 \theta_w$ ,  $\sin^2 \theta_w \approx 0.23$ ,  $\sigma = 1.76 \times 10^{-44}$  cm $^2$ , and  $\alpha = 1.25$  (Shapiro & Teukolsky 1983) and the rest of the symbols have their usual meanings.

To compute the internal energy, cooling rate, and pressure due to neutrinos we used a two-stream approximation (Popham & Narayan 1995; Di Matteo, Perna & Narayan 2002; Janiuk, Yuan, Perna & Di Matteo 2007):

$$E_\nu(\tau) = 3P_\nu(\tau) = \frac{7\pi^2(k_{\text{B}}T)^4}{8 \cdot 15(\hbar c)^3} \left( \frac{(\tau_{\text{abs}} + \tau_{\text{scat}})/2 + 1/\sqrt{3}}{(\tau_{\text{abs}} + \tau_{\text{scat}})/2 + 1/\sqrt{3} + 1/3\tau_{\text{abs}}} \right) \text{ erg cm}^{-3}, \quad (5)$$

$$\dot{q}_\nu(\tau) = \frac{7}{8} \left( \frac{4\sigma_{\text{SB}}T^4/3}{(\tau_{\text{abs}} + \tau_{\text{scat}})/2 + 1/\sqrt{3} + 1/3\tau_{\text{abs}}} \right) \left( \frac{H}{\text{cm}} \right) \text{ erg cm}^{-3} \text{ s}^{-1}, \quad (6)$$

and

$$P_\nu(\tau) = \frac{1}{3} \left( \frac{7\pi^2(k_{\text{B}}T)^4}{8 \cdot 15(\hbar c)^3} \right) \left( \frac{(\tau_{\text{abs}} + \tau_{\text{scat}})/2 + 1/\sqrt{3}}{(\tau_{\text{abs}} + \tau_{\text{scat}})/2 + 1/\sqrt{3} + 1/3\tau_{\text{abs}}} \right). \quad (7)$$

The total neutrino luminosity (in erg s $^{-1}$ ) is then calculated through

$$L(\tau) = \int \dot{q}_\nu(\tau) dV \text{ erg s}^{-1}. \quad (8)$$

## 2.2. Initial setup and numerical method

Our initial data were taken from the one-dimensional pre-SN calculations of Woosley & Heger (2006). Specifically we considered model 16TI, a rapidly rotating ( $v_{\text{rot}} = 390$  km s $^{-1}$  at the equator),  $16 M_\odot$  WR star of low metallicity (1% solar), low mass loss ( $2 M_\odot$  loss at the end of the evolution), with an iron core surrounded by silicon and oxygen, neon and carbon shells. The density, temperature, and radial velocity distributions as functions of the spherical radius,  $R$ , were mapped onto a two-dimensional configuration assuming spherical symmetry. We further suppose that the low angular momentum iron core (with mass  $M_{Fe} = 1.6 M_\odot$ ) will promptly collapse to a BH (possibly producing a

<sup>1</sup> Neutrino emission through plasmon decays and nucleon–nucleon bremsstrahlung was also computed and found to be insignificant compared to capture and annihilation.

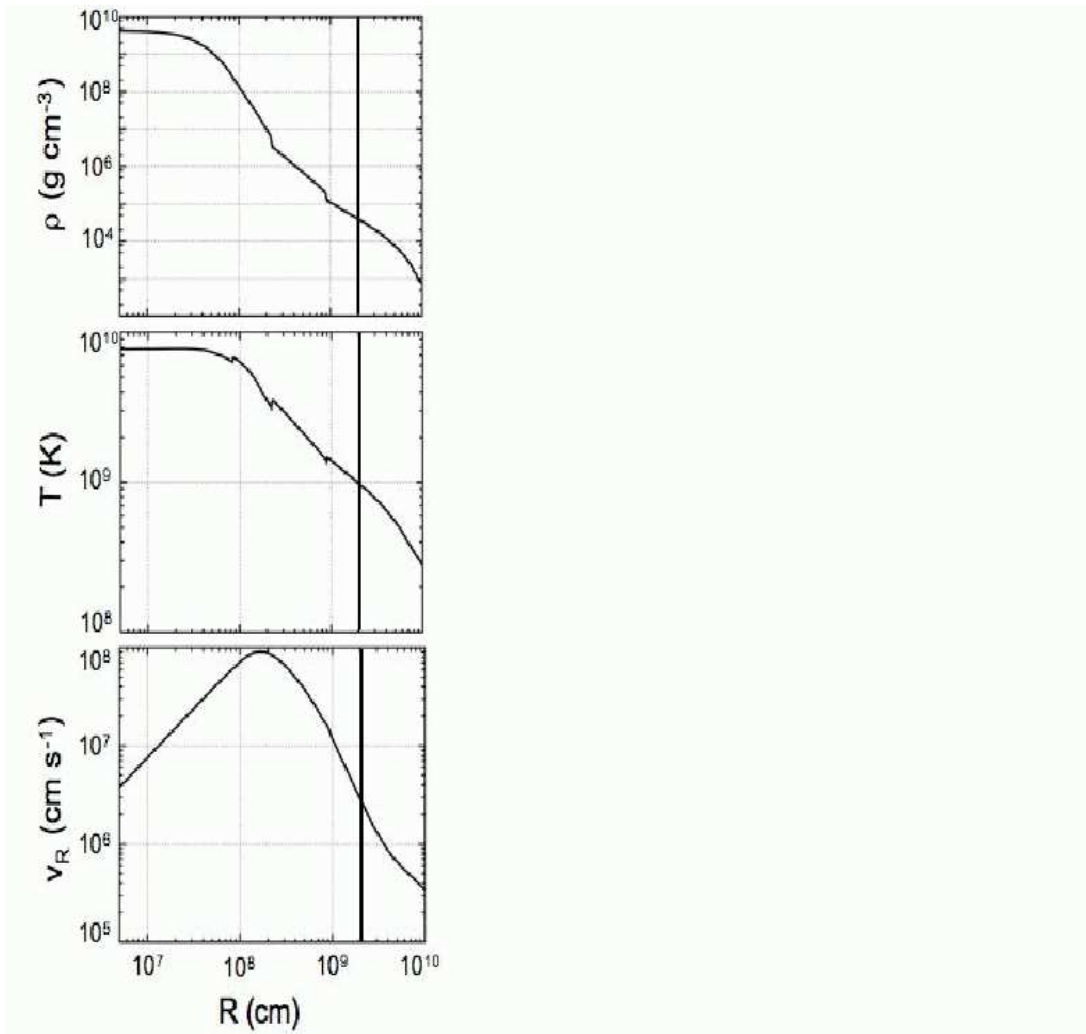


FIG. 1.— Density, temperature and radial velocity profiles in the pre-SN star used as an initial condition (model 16TI of Woosley & Heger (2006)). The solid vertical line in each panel marks the outer computational boundary used in the simulations.

Type I collapsar, see Section 1) and thus condense all of this matter onto the origin in a point mass at the start of the simulation, when the surrounding envelope begins its infall.

The calculations are performed with a two-dimensional Smooth Particle Hydrodynamics (SPH) code (Monaghan 1992) in cylindrical coordinates  $(r, z)$  with azimuthal symmetry (Lee & Ramirez-Ruiz 2002, 2006; Lee, Ramirez-Ruiz & Page 2005) and a reflecting boundary along the polar axis (no reflection about the  $z = 0$  plane is assumed). The inner and outer boundaries were set at spherical radii  $R_{\text{in}} = 2 \times 10^6$  cm and  $R_{\text{out}} = 2 \times 10^9$  cm, respectively, with free outflow conditions imposed during the simulation. Any material crossing the inner boundary is assumed to be accreted by the BH, whose mass is correspondingly updated. Matter lost through the outer boundary is not followed. We solved the continuity, momentum, and energy equations, including the terms arising from the full viscous stress tensor  $t_{r\phi}$  (Lee & Ramirez-Ruiz 2002), and took the  $\alpha$  prescription (Shakura & Sunyaev 1973) for the coefficient of viscosity,  $\eta_v = \alpha \rho c_s H$ , where  $c_s$  is the local sound speed and  $H = c_s / \Omega_K$  is the pressure scale height ( $\Omega_K$  is the local Keplerian orbital angular frequency). Doing the calculation in two dimensions allows for good spatial resolution, a considerable simulated interval and a solid discussion of angular momentum and viscosity effects. The initial profile is reproduced with a Monte Carlo accept/reject procedure, typically with  $1 - 2 \times 10^5$  SPH particles in the computational domain. The spatial resolution is intrinsically adaptive in this numerical scheme and varies greatly, increasing at small radii (or equivalently, high densities) with a typical smoothing length of few  $\times 100$  m in the inner disks formed.

The gravitational potential of the BH is computed with the pseudo-Newtonian expression of Paczyński & Wiita (1980):

$$\phi = -\frac{GM_{\text{BH}}}{r - r_g}, \quad (9)$$

which approximates GR effects in the inner regions for a nonrotating (Schwarzschild) BH. In particular, it reproduces

the position of the innermost stable circular orbit at  $r_{isco} = 3r_g$ , as well as the marginally bound orbit at  $r_{mb} = 2r_g$ .

The mass in the collapsing envelope is comparable to that of the BH, so one should consider self-gravity. We assume that the mass distribution remains roughly spherical, so a mass element at spherical radius  $R_0$  is affected only by the matter distribution at radii  $R \leq R_0$  as if it were concentrated at the center of the star. This, while strictly valid only for configurations with spherical symmetry, is nevertheless a good approximation for the present set of calculations, since deviations in the mass distribution indeed remain small. Figure 1 shows the initial density, temperature, and radial velocity profiles in the pre-SN star as functions of spherical radius, taken from Woosley & Heger (2006).

### 3. RESULTS

#### 3.1. Expectations

Consider a nonrotating BH surrounded by rotating material distributed in spherical symmetry with vanishing pressure. For a distribution of specific angular momentum increasing monotonically with respect to the polar angle, flowlines in the polar regions will be qualitatively different than those near the equator, and can be divided into three types: (1) those with very little angular momentum, moving nearly radially into the BH; (2) those with high angular momentum which can find a point where centrifugal support balances the gravitational field (the circularization radius); and (3) those that would accrete onto the central mass but cross the equatorial plane,  $z = 0$ , before doing so. Recall that in GR capture orbits exist even for nonvanishing angular momentum, and the critical value defining this class of solutions is  $J_{\text{crit}} \simeq 2.0r_g c$ . Here we will consider  $J \geq J_{\text{crit}}$  as high angular momentum, and  $J \sim J_{\text{crit}}$  as low. This general situation has been considered before in the context of LMXBs by Beloborodov & Illarionov (2001), and for accretion modes in collapsars by Lee & Ramirez-Ruiz (2006) (an analytical derivation of low angular momentum flow lines in GR has been carried out by Mendoza et al. (2009)).

Encountering the centrifugal barrier or a flowline from the opposite hemisphere can lead to a shock (and thus hydrodynamical effects) in which the kinetic energy is efficiently converted into thermal energy. If the material does not have enough angular momentum to remain in orbit, it will fall onto the BH due to GR effects, *even in the absence of any angular momentum transport mechanism* through a fast, nearly *inviscid* disk. For high angular momentum, a disk (with scale height  $H$  and typical radius  $r$ ) forms in the equatorial plane, and if cooling occurs some of this energy will be lost from the system through photons or neutrinos, depending on the physical conditions. For efficient cooling the disk will be nearly isothermal and geometrically thin, with  $H \ll r$ . In the opposite adiabatic regime it can be quite thick, and  $H \sim r$ . Energy dissipation will in general circularize motions at a radius given by the local value of angular momentum, and if any of this is subsequently removed (through any mechanism), or it is already below the critical value, the material inside the disk may move radially and possibly be accreted by the BH. The size and geometry of the newly formed disk thus reflects: (1) the angular momentum distribution, fixing the point where the centrifugal barrier is encountered; (2) the mass accretion rate, giving the total gravitational energy which can be converted into thermal energy; (3) the cooling rate, determining the disk geometry; (4) the value of the  $\alpha$  parameter, responsible for angular momentum transport.

In general, previous collapsar studies or neutrino-dominated accretion flow studies have considered cases where  $J \gg J_{\text{crit}}$  (MacFadyen & Woosley 1999; Popham, Woosley & Fryer 1999; Heger et al. 2000; Narayan, Piran & Kumar 2001; Proga & Begelman 2003; Proga, MacFadyen, Armitage & Begelman 2003). Only recently has the low angular momentum regime in the collapsar context been addressed (Lee & Ramirez-Ruiz 2006), showing the presence of the small *dwarf* disk as described above. For  $J > 2.0r_g c$ , a thick disk forms, supplying the bulk of the neutrino luminosity from a shocked toroidal region around the BH. More recently, Janiuk & Proga (2008) considered the minimum angular momentum required for disk formation, taking into account that the accretion of mass by the central object raises the angular momentum threshold as the stellar core collapses.

We explored the dynamical evolution for different values of the  $\alpha$  viscosity parameter (see Table 1), and more importantly, different values of angular momentum, which were always separated into radial,  $R$ , and polar angle,  $\theta$  (measured from the rotation axis), variations as  $J = J(R, \theta) = J_R(R) J_\theta(\theta)$ . For the radial component,  $J_R(R)$ , we considered constant values with radius (see Table 1). We will consider more realistic distributions of  $J_R(R)$  in future work (D. Lopez-Camara et al. 2008, in preparation). In all cases the initial distribution for  $J(\theta)$  corresponded to rigid body rotation on shells,  $J(\theta) = \sin^2 \theta$ .

#### 3.2. Global properties and flow morphology

For  $J(R) = 2.0r_g c$ , the flow is essentially at the critical value, and remains nearly radial. Even though some compression occurs in the equatorial region the centrifugal barrier is absent and no shocks are formed. Moreover, since  $J(R)$  is constant, the initial velocity field and density map (shown in Figure 2) do not vary substantially as the simulation progresses. For an inflow in strict free fall, conservation of mass and energy give a density profile

$$\rho = \frac{\dot{M}}{4\pi r^2 v_r} = 1.2 \times 10^8 \left( \frac{\dot{M}}{0.5 M_\odot \text{ s}^{-1}} \right) \left( \frac{r}{10^7 \text{ cm}} \right)^{-3/2} \left( \frac{M_{\text{BH}}}{1.7 M_\odot} \right)^{-1/2} \text{ g cm}^{-3}, \quad (10)$$

where  $\dot{M}$  is the mass accretion rate and  $M_{\text{BH}}$  the BH mass. The solution is plotted as a dotted line in Figure 3 with the above scalings set to unity, clearly showing the excellent agreement between the full simulation and this simple estimate along the equator. The energy release, however, is not negligible, as will be seen below in Section 3.5. As

TABLE 1  
MODEL PARAMETERS

$J_0$	$\alpha$ ( $r_g c$ )
2.0	0.10
2.5	0.10
3.0	0.10
2.0	0.01
2.5	0.01
3.0	0.01
2.0	0.00
2.5	0.00
3.0	0.00

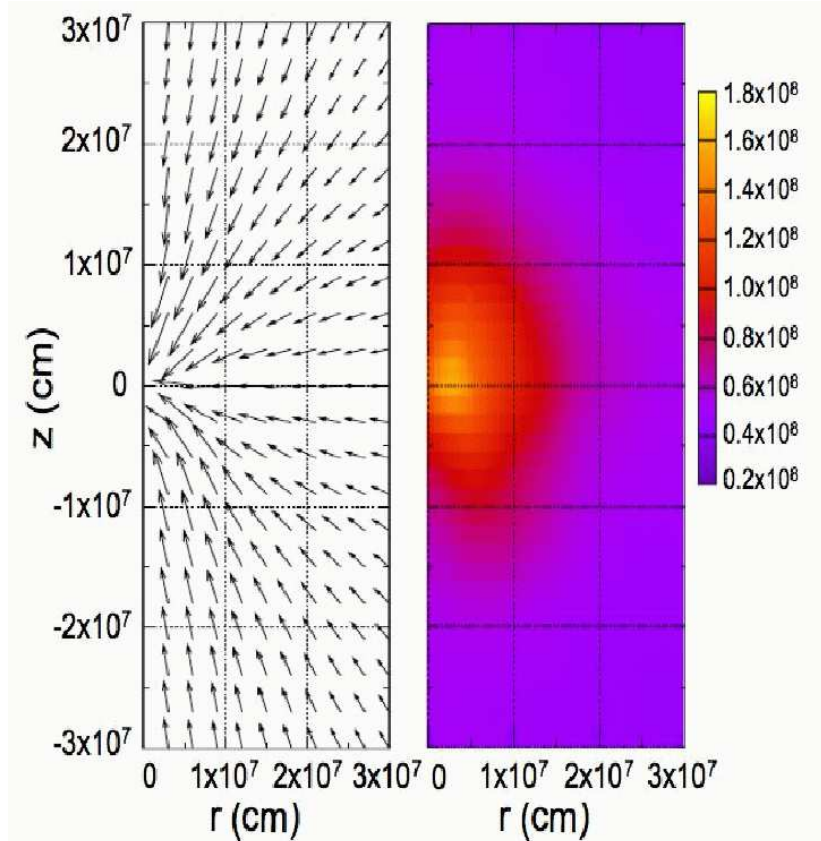


FIG. 2.— Velocity field and density map (in  $\text{g cm}^{-3}$ ) for  $(J_0, \alpha) = (2r_g c, 0.1)$  at  $t = 0.2$  s. The largest vector corresponds to  $v \approx 8 \times 10^7$   $\text{cm s}^{-1}$ .

long as the equatorial angular momentum is below this critical value, the solution is insensitive to the actual value of the viscosity parameter,  $\alpha$ , that is chosen (we computed solutions for  $\alpha$  in the range  $0 - 10^{-1}$ ).

For values of  $J(R)$  above the critical value the outcome changes drastically. The scale of the disk correlates with  $J_0$  so we will limit the discussion to the case with  $J(R) = 3.0r_g c$  and  $\alpha = 0.10$ . An initial disk forms close to the equator after 0.1 s, the free-fall time from the boundary of the Fe core, when the innermost regions of the envelope approach their circularization radius  $r_c \approx J_0^2/GM_{\text{BH}}$ . The transformation of kinetic into thermal energy at the centrifugal barrier produces a hot torus around the BH. Figure 4 shows the velocity field and a density map at  $t = 0.2$  s for  $(J_0, \alpha) = (3r_g c, 0.1)$ . Note how in the velocity field the flow lines in the polar regions are still largely radial, and an asymmetry is apparent, with the polar shock lying substantially closer to the black hole than in the equator. A large-scale meridional circulation with two prominent eddies is also apparent.

The temperature and density rise rapidly behind the shock front, releasing a substantial amount of energy and photodisintegrating He. It is here where neutrino emission, finite optical depth effects and neutronization can become important. A substantial fraction of the released energy will likely be directed to the polar regions because of geometrical effects, and may give rise to a fireball capable of producing a GRB (see Section 3.5).

Outside the shock front, the solution is essentially the same as for low angular momentum (see Figure 3), with a

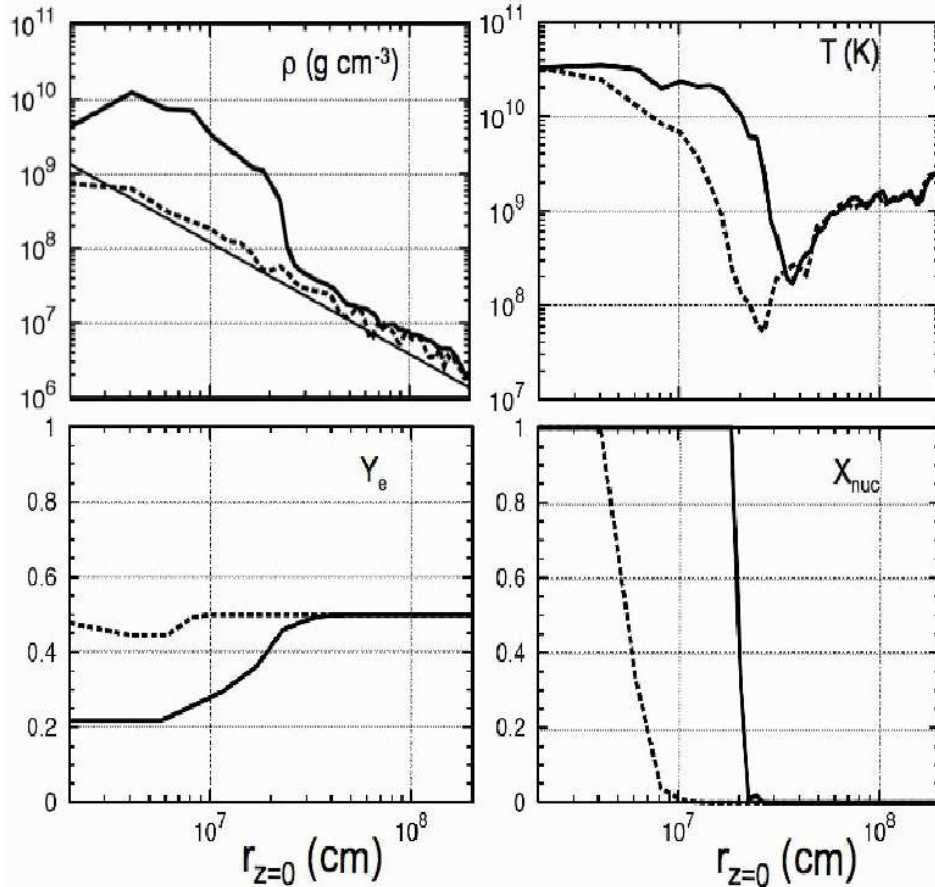


FIG. 3.— Equatorial ( $z = 0$ ) density, temperature, electron fraction and nucleon mass fraction distribution for  $(J_0, \alpha) = (3r_g c, 0.1)$  (solid line) and  $(J_0, \alpha) = (2r_g c, 0.1)$  (dashed line) at  $t = 0.2$  s. The power law given by a thin solid line in the density panel is the solution given in Equation (10).

jump at  $r \approx r_c$ . For angular momentum  $J_0 = Ar_g c$ , with  $A \geq 2$  being a constant, the circularization radius for equatorial matter is  $r_c \approx 2A^2 r_g$  and the free-fall velocity at  $r_c$  is  $v_{\text{ff}} = c/2^{1/2}A$ . If the kinetic energy of infall is entirely transformed into thermal energy, one would naively estimate the latter as

$$kT = \frac{m_p c^2}{12A^2} \approx 10(A/3)^{-2} \text{MeV}. \quad (11)$$

This is clearly an overestimate of the temperature, since the velocity is not entirely radial but has a substantial azimuthal component,  $v_\phi$ , by the time it reaches the circularization radius,  $r_c$ . It does nevertheless give a useful estimate (and upper bound) on the postshock temperature, as can be seen from Figure 3. As we shall see, it is also high enough to guarantee the complete photodisintegration of the infalling nuclei into their constituent neutrons and protons.

In the initially small disk that forms at the centrifugal barrier, if  $\alpha \neq 0$  transport processes transform the constant distribution of angular momentum into a nearly Keplerian one where differential rotation is important. For the Newtonian case the orbital frequency is  $\Omega \propto r^{-3/2}$  and at a few gravitational radii this is not a bad approximation even in the pseudo-GR PW potential. In a way this partially erases the memory of the initial distribution: as long as the rotation rate is above a certain threshold, the inner disk will quickly converge to a centrifugally supported structure with strong differential rotation, independently of the details of the initial angular momentum profile. The associated shear produces dissipation and pumps mechanical energy into thermal energy. The rotational structure of the inner disk depends on whether  $\alpha$  is finite or not. If  $\alpha \neq 0$  the actual value of the specific angular momentum can grow beyond the initial equatorial value  $J_0$  through transport. For the inviscid regime,  $\Omega \propto r^{-3/2}$  (and hence  $J \propto r^{1/2}$ ) only as long as this implies  $J \leq J_0$ . At greater radii the equatorial flow maintains constant specific angular momentum.

Approximately 0.2 seconds after the formation of the initial disk, a shock begins to propagate outward, initially moving at  $v \approx 2 \times 10^8$  cm s $^{-1}$  in the equatorial regions. The postshock gas pushes out against the infalling envelope

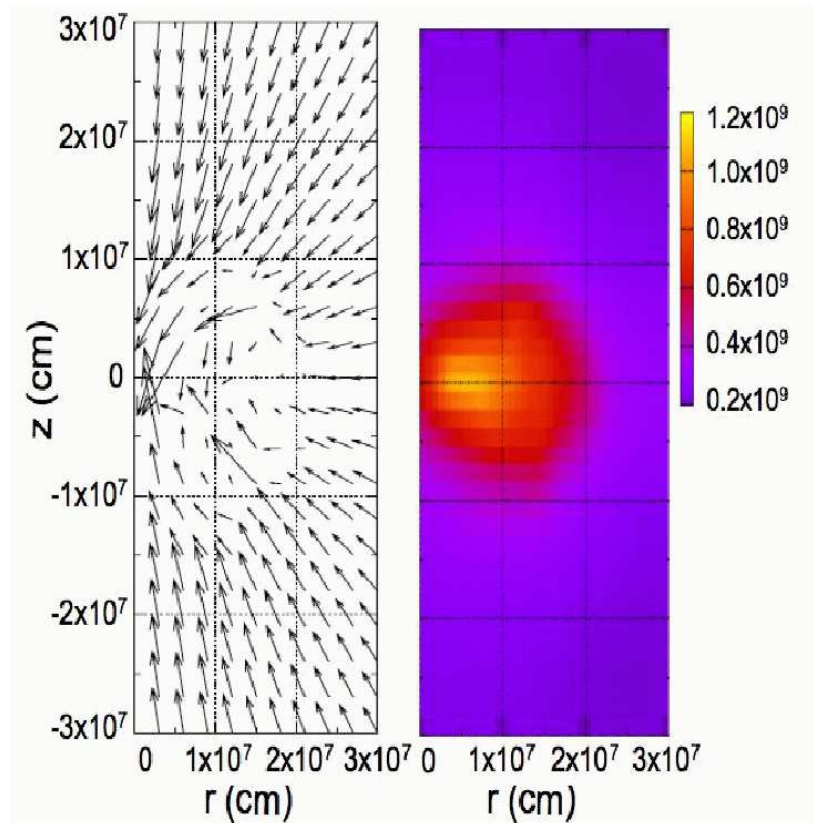


FIG. 4.— Velocity field and density map (in  $\text{g cm}^{-3}$ ) for  $(J_0, \alpha) = (3r_{\text{gc}}, 0.1)$  at  $t = 0.2$  s. The largest vector corresponds to  $v \approx 8 \times 10^7$   $\text{cm s}^{-1}$  for densities lower than  $5 \times 10^8$   $\text{g cm}^{-3}$ . At higher values the velocity vectors are reduced by a factor of two. The location of the accretion shock is clearly seen at  $r(z=0) \approx 2 \times 10^7$  cm.

mainly because of viscous heating for  $\alpha = 0.1$ , and is aided by a combination of neutrino heating and He synthesis<sup>2</sup>. The calculations were stopped at  $t \sim 0.5$  s, when the shock reached the outer boundary. Not only is the numerical solution no longer self-consistent, but by then our resolution had decreased notably, since accretion onto the BH entails a loss of particles, and thus resolution. We will address this issue in an adaptive form in future work. For low viscosity the inner disk is denser due to the reduced transport efficiency and the outward motion of the shock is only slightly delayed. In the inviscid limit there is no associated heating but the piling up of material due to the lack of transport also induces outward motion of the shock front after a comparable delay of  $\simeq 0.2$  s.

In general, the inner disk can remain thick despite the presence of cooling because of the continuous infall of material and, in some cases, because the optical depth to neutrinos is large enough to keep the internal energy from immediately escaping. As long as the angular momentum of the infalling gas is greater than the critical value, the morphology is similar, with a greater radial extent for higher  $J_0$ .

The breaking of spherical symmetry is in principle a problem for the computation of self-gravity, described in Section 2.2. We thus checked how far the actual flow departs from spherical symmetry in terms of the mass distribution as a function of the polar angle  $\theta$ , and find that the scatter in the radially integrated mass along cones with constant  $\theta$  is small enough (10%) to be ignored in a first treatment.

### 3.3. The importance of cooling

To highlight and better understand the importance that the proper computation of cooling has on the global properties of the solution, we have calculated the evolution of the flow in two simplified cases. Since neutrinos are the only means other than advection onto the BH through which the gas can cool, and thus move lower in the gravitational potential well, there are two limits in this respect: adiabatic inflow, in which no cooling occurs, and isothermal flow, in which on the contrary, it is extremely efficient. The true solution must lie somewhere between these two extremes, and it is instructive to know which it resembles the most. We computed these, in one case by eliminating the cooling terms in the energy equation and thus impeding the outward flow of energy through neutrinos, and in the other by using an ideal gas equation of state with  $P = (\gamma - 1)\rho v$ , where  $\gamma = 1.01$  and the same initial conditions, thus mimicking the isothermal case where  $\gamma = 1$  and compressibility is very high. The velocity fields and the corresponding density maps (also for  $J_0 = 3r_{\text{gc}}$  and  $\alpha = 0.1$  are shown in Figures 5 and 6. Equatorial density profiles for the various cases are shown in Figure 7, and can be compared with those in Figure 2). The isothermal flow looks qualitatively similar to the low

<sup>2</sup> In a test calculation with the viscous heating terms switched off, the shock had not started to move outward after 0.5 seconds.

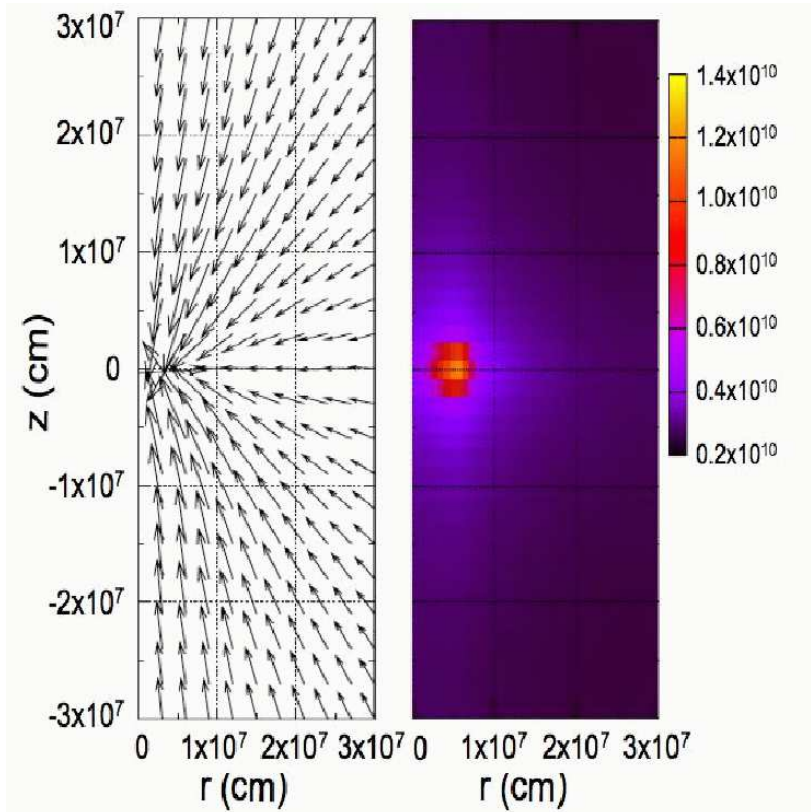


FIG. 5.— Velocity field and density map (in  $\text{g cm}^{-3}$ ) for isothermal flow with  $J_0 = 3r_g c$  and  $\alpha = 0.1$  at  $t = 0.2$  s.

angular momentum case, but the density is 2 orders of magnitude larger. There is little temporal evolution once the centrifugal barrier is reached, and the solution is quasi-stationary. On the other hand, in the adiabatic solution as soon as the infalling gas reaches the centrifugal barrier, the shock bounces rapidly outward and the subsequent expansion produces a strong flow reversal, sweeping the inner envelope outward and beyond the outer boundary (compare with Figure 4 and note that the spatial scale is 5 times larger). At the instant shown in Figure 7 the density has decreased considerably, even beyond the solution where neutrino emission was included. The fact that the accretion disk remains geometrically thick in the calculation with neutrino cooling indicates that it is not extremely efficient, resembling the adiabatic solution qualitatively, but significant enough to avoid such a prompt outflow. Given that the emissivities are sensitive functions of temperature and composition, an accurate expression for these and at least an approximate treatment of neutrino optical depths is clearly a crucial ingredient in the evolution. Note that since the optical depth to neutrinos is never extremely large, once emitted they are relatively free to escape and are not advected with the flow.

### 3.4. Thermodynamics inside the disk

The origin of the energy release and the associated neutrino luminosity can be easily understood by examining the various emission mechanisms separately. Figure 8 shows a snapshot at  $t = 0.2$  s of the neutrino emissivities for pair annihilation ( $\dot{q}_{ann}$ ) and  $e^\pm$  capture onto free nucleons ( $\dot{q}_{cap}$ ) as a function of the cylindrical radius  $r$  in the equatorial plane ( $z=0$ ), for  $(J_0, \alpha) = (3r_g c, 0.1)$ .

The highest energy release occurs very close to the BH: at  $r \leq 2 \times 10^7$  cm both  $\dot{q}_{cap}$  and  $\dot{q}_{ann}$  rise at least 3 orders of magnitude and release up to  $10^{18}$   $\text{erg s}^{-1} \text{cm}^{-3}$ . The figure also shows the corresponding optical depth contributions for both processes as well as coherent scattering ( $\tau_{scat}$ ) for  $(J_0, \alpha) = (3r_g c, 0.1)$  at  $t = 0.2$  s. The inner regions ( $r \leq 2 \times 10^7$  cm) can become somewhat opaque while at large radii the fluid remains optically thin. Electron/positron annihilation dominate the optical depth in the dense inner region over captures onto free nucleons and coherent scattering. Neutrinos are not entirely free to escape and corrections due to finite optical depth both in the pressure and luminosity (Eq. 6) must be taken into account. A clue to the disk's structure can be inferred from the comparison of the local cooling (or Kelvin-Helmholtz) time,  $t_{cool} \approx E/\dot{q}_\nu$  to the dynamical time,  $t_{dyn} \approx (GM_{BH}/r^3)^{-1/2}$ , plotted in Figure 9. Despite the high accretion rates, even in the inner regions the cooling time is much longer than the orbital period<sup>3</sup>. This is in agreement with the previous comparison to the isothermal and adiabatic limits in Section 3.3, where we already found that qualitatively at least, the overall picture is indicative of inefficient cooling.

<sup>3</sup> At large radii it is appropriately even larger, since the stellar envelope is essentially in hydrostatic equilibrium.

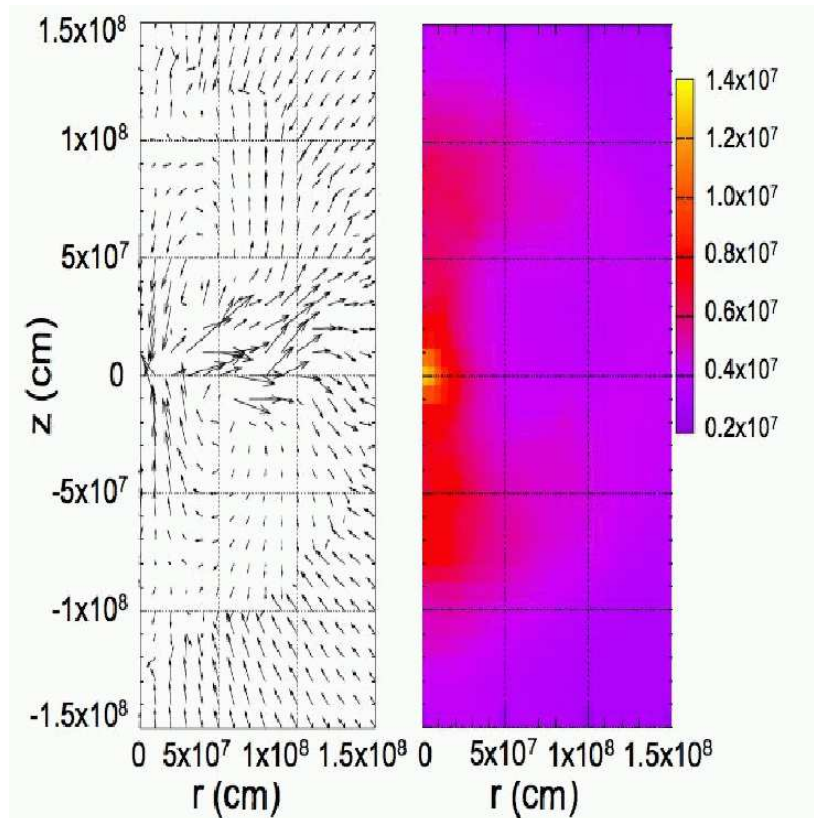


FIG. 6.— Velocity field and density map (in  $\text{g cm}^{-3}$ ) for adiabatic flow with  $J_0 = 3r_{\text{gc}}$  and  $\alpha = 0.1$  at  $t = 0.2$  s. Note the different spatial scale compared to the previous figures. The largest velocity vectors correspond to  $10^8 \text{ cm s}^{-1}$  for densities lower than  $5 \times 10^7 \text{ g cm}^{-3}$ . At higher values the vectors are reduced by a factor of 2.

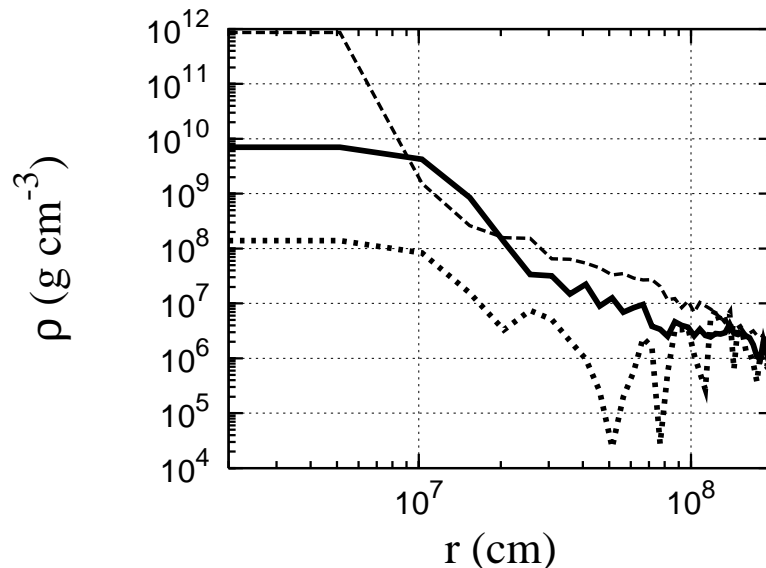


FIG. 7.— Equatorial ( $z = 0$ ) density distributions at  $t = 0.2$  s for the simulations carried out in the adiabatic (dotted) and isothermal (dashed) limits, both for  $(J_0, \alpha) = (3r_{\text{gc}}, 0.1)$ . The thick solid line is the simulation with full microphysical treatment and  $(J_0, \alpha) = (3r_{\text{gc}}, 0.1)$ .

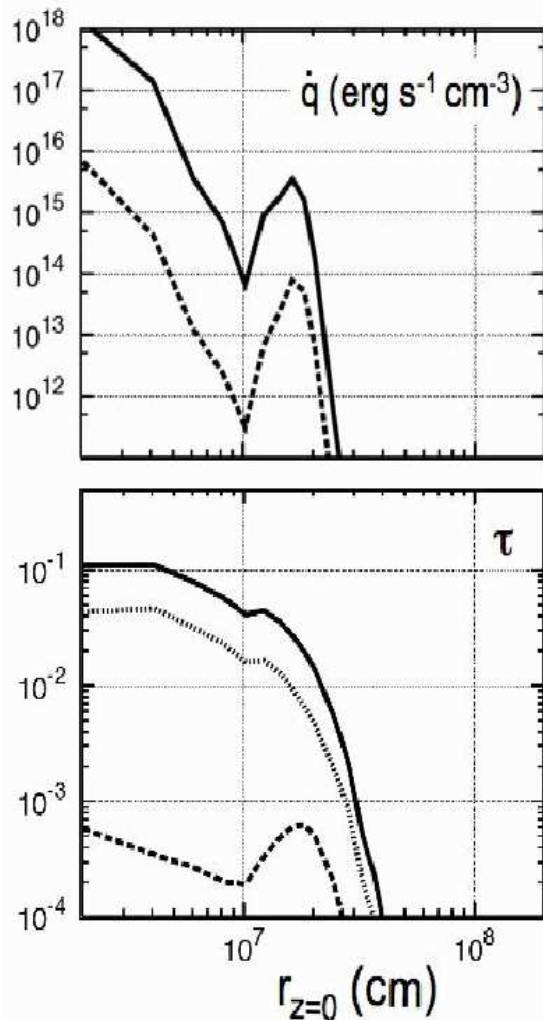


FIG. 8.— Upper panel: neutrino emissivities  $\dot{q}_{ann}$  (solid line) and  $\dot{q}_{cap}$  (dashed line) for  $(J_0, \alpha) = (3r_g c, 0.1)$  at  $t = 0.2$  s. Lower panel: the corresponding optical depth contributions from  $\tau_{abs-ann}$  (solid line),  $\tau_{abs-cap}$  (dashed line),  $\tau_{scat}$  (dotted line) for  $(J_0, \alpha) = (3r_g c, 0.1)$  at  $t = 0.2$  s.

Regarding the thermodynamical properties of the flow, we will focus on  $(J_0, \alpha) = (3r_g c, 0.1)$  and  $(J_0, \alpha) = (2r_g c, 0.1)$  (the remaining cases are quite similar). Equatorial ( $z = 0$ ) profiles for density, temperature, electron fraction and nucleon mass fraction are shown in Figure 3 for both runs. The outwardly moving accretion shock front in the high angular momentum case is visible at  $r \approx 2 \times 10^7$  cm. Once in the postshock region, compression and the rise in temperature fully break up  $\alpha$  particles into their constituent neutrons and protons. The consequent cooling through  $e^\pm$  captures onto neutrons and protons allows the gas to reach densities high enough that neutronization takes place, lowering  $Y_e$  to minimum values close to 0.2 (the higher densities also make the fluid become more degenerate).

For the calculation with  $J(R) = J_{crit}$  no centrifugally supported disk forms, although compression is important in the flow just before the gas falls through the inner boundary. The equatorial profiles (shown in the previous figures along with those for  $J_0 = 3.0r_g c$ ) show little evolution, and this case is basically in the inviscid limit, where varying  $\alpha$  makes little or no difference on the outcome. The gas is so close to being in free fall that the much longer viscous timescale becomes irrelevant, and runs with different values of  $\alpha$  yielded the same solution.

Contrary to the cases with  $J(R) > J_{crit}$ , where the disk was in some cases opaque, the maximum optical depth is now at most  $\tau = 0.01$ , dominated also by pair annihilation (the temperature is  $kT \simeq 4$  MeV) and the emissivities are substantially lower. Compression and the associated rise in temperature are strong enough to dissociate He almost completely in the inner regions, but no significant neutronization occurs because the maximum density is only  $\simeq 10^9$  g cm $^{-3}$ . Very close to the BH,  $e^\pm$  captures produce slight neutronization and the electron fraction drops down to  $Y_e = 0.45$ . The  $e^\pm$  pairs are at the threshold of degeneracy, with  $\mu_e/k_B T \approx 1.5$ , where  $\mu_e$  is the chemical potential of the electrons.

The possibility of this transition at high accretion rates (of order a few tenths of a solar mass per second here) was hinted at in the simpler calculations of Lee & Ramirez-Ruiz (2006), but the equation of state used there did not

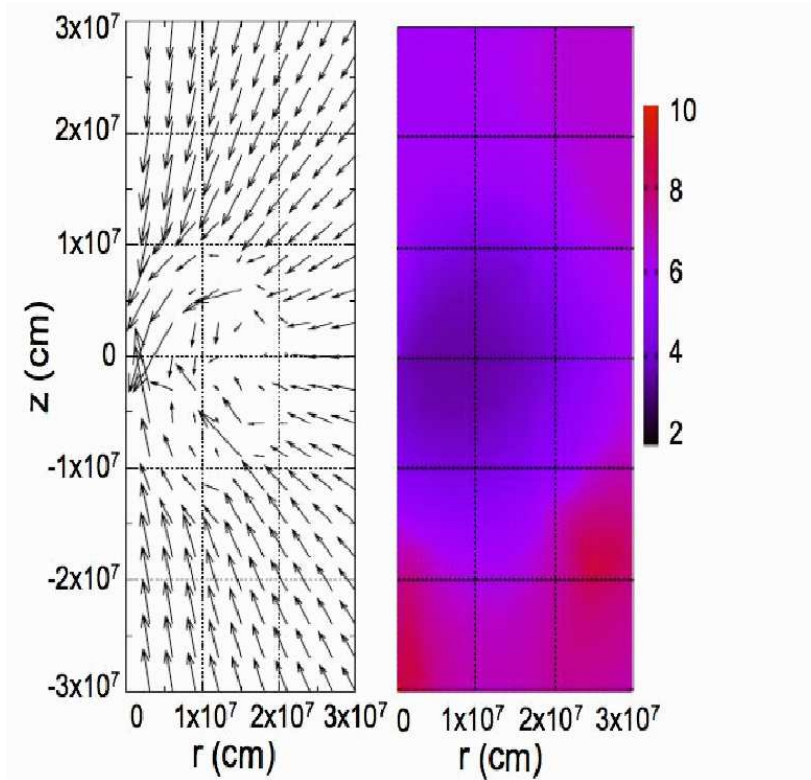


FIG. 9.— Map of  $\log_{10}(t_{cool}/t_{dyn})$  for  $(J_0, \alpha) = (3r_g c, 0.1)$  at  $t = 0.2$  s. For the velocity field, the largest vectors are the same as in Figure 4.

TABLE 2  
NEUTRINO ENERGETICS

$J_0$ ( $r_g c$ )	$\alpha$	$\rho_{10}$	$T_{10}$	$Y_e$	$E_{ann}$ (MeV)	$E_{cap}$ (MeV)
2.0	0.10	0.07	3.70	0.44	12.76	2.87
2.5	0.10	1.02	4.20	0.23	14.46	5.52
3.0	0.10	0.82	3.48	0.18	12.00	4.74
3.0	0.01	4.00	3.75	0.10	12.94	6.63
3.0	0.00	1.89	4.87	0.12	16.77	5.48

permit neutronization or degeneracy effects to play a role<sup>4</sup>. It is clear from the present set of calculations that such approximations are valid only for quite lower accretion rates (a few hundredths of a solar mass per second). This limitation is valid also for other collapsar studies, where neither finite degeneracy or neutronization have been fully considered. Two important potential consequences in this context stand out.

First, the energy of a given neutrino depends on the physical process responsible for its creation. Those arising from pair annihilation (a thermal process) have characteristic energies of the order  $E_{ann} \approx 4kT$ , while those due to  $e^\pm$  capture onto free nucleons (a weak interaction) have energies of the order  $E_{cap} \approx E_F$ , where  $E_F \approx 9(\rho_{10} Y_e)^{1/3}$  MeV is the Fermi energy of electrons/positrons ( $\rho_{10} = \rho/10^{10}$  g cm<sup>-3</sup>). Table 2 shows the values for  $\rho_{10}$ ,  $T_{10}$ ,  $Y_e$ ,  $E_{ann}$ , and  $E_{cap}$  for our calculations (in the inner regions where the energy release is largest, i.e., where  $\rho = \rho_{max}$ ,  $T = T_{max}$ , and  $Y_e = Y_{e,min}$ ). As  $E_{ann}$  and  $E_{cap}$  vary with respect to  $J_0$  and  $\alpha$ , the transition to a different thermodynamic regime will thus modify the emergent neutrino spectrum. This in turn affects the global energy release, since at a given neutrino luminosity,  $L_\nu$ , the efficiency for neutrino annihilation scales with  $\langle E_\nu \rangle$ , and thus more energetic neutrinos will be more efficiently converted into a relativistic pair plasma.

Second, the morphology of the flow may be influenced by the available energy sinks (e.g., advection, neutrino losses) allowed in a calculation. Dissipation in the disk through viscosity adds to the internal energy reservoir. If it is allowed to escape with moderate efficiency the vertical scale height will be limited. Otherwise the disk will tend to expand in response, or possibly drive winds from its surface. In the original collapsar calculation of MacFadyen & Woosley (1999), strong winds driven from the surface of the disk at small radii were reported for one calculation, with  $\alpha = 0.10$ .

<sup>4</sup> They assumed that hot  $e^\pm$  pairs were abundant, producing a pressure contribution  $\propto T^4$ , and that  $\tau_\nu \ll 1$ .

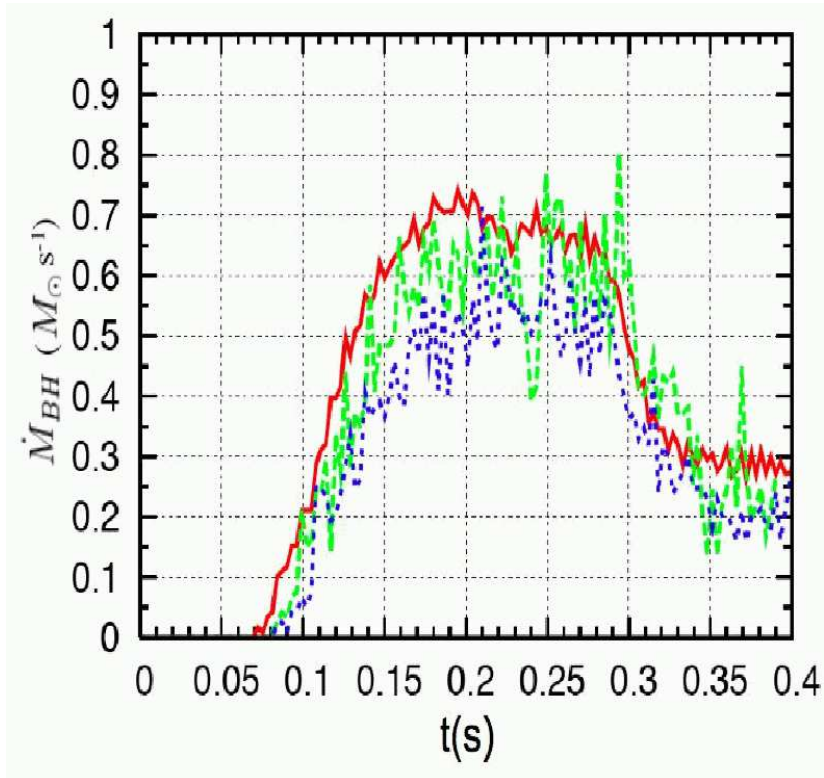


FIG. 10.— Mass accretion rate onto the BH ( $\dot{M}_{BH}$ ) for a fixed  $\alpha$  with different angular momentum values:  $(J_0, \alpha) = (2r_{gc}, 0.1)$  (red solid line),  $(J_0, \alpha) = (2.5r_{gc}, 0.1)$  (green dashed line), and  $(J_0, \alpha) = (3r_{gc}, 0.1)$  (blue dotted line).

Calculations with a smaller dissipation rate did not exhibit this feature. For now, our computations do not span such a long time interval, but the essential morphological features (expanding outer accretion shock, hot torus, and dense inner disk) are well established by 0.4 s. We intend to further explore these issues in a second set of simulations with varying angular momentum distributions. Any potential outflows emanating from the inner regions could have a significant impact on the observable signature of the stellar collapse, and so this deserves careful consideration.

### 3.5. Accretion rate, neutrino luminosity, and energy conversion efficiency.

The mass accretion rate  $\dot{M}_{BH}(t)$  was computed at the inner boundary  $R = R_{in} = 20$  km and is shown in Figure 10 for three runs with the same value of  $\alpha = 0.10$ , and different angular momentum  $J_0$ . The corresponding neutrino luminosity is plotted in the top panel of Figure 11. The initial delay of about 0.1 seconds represents the infall time from the outer boundary of the iron core. Thereafter the accretion rate and the luminosity rise rapidly, reaching approximately 0.6 solar masses per second and  $10^{51} - 10^{52}$  erg  $s^{-1}$  respectively. The inner disk is responsible for most of the energy release, and its formation and steady configuration for the next 0.1-0.2 seconds produce a nearly constant accretion rate and luminosity. The efficiency  $L_{\nu}/\dot{M}_{BH}c^2$  during this period is approximately 0.01 and 0.001, for high and low angular momentum, respectively, reflecting the increased importance of advection when the flow is quasi-radial. Note that despite the absence of a centrifugal barrier and a dense disk, the configuration with low angular momentum is capable of significant energy release ( $L_{\nu} \simeq 10^{51}$  erg  $s^{-1}$ ).

The launching of the accretion shock after a few tenths of a second leads to a drop in both the accretion rate and the luminosity, while maintaining a nearly constant efficiency. For  $J_0/(r_{gc}) = 2.5, 3.0$  the outwardly propagating shock eventually perturbs the mass flux to the inner disk before reaching the outer boundary used in the calculation. The higher mass accretion rate at low angular momentum (below the critical value) is due to GR effects but does not initially translate into a higher luminosity because the material falls nearly radially into the BH and is unable to radiate efficiently.

Neutrino luminosities for a fixed value of angular momentum ( $J_0 = 3.0r_{gc}$ ) and varying efficiency of viscous transport are shown in the bottom panel of Figure 11. A moderate to null viscosity is in this early stage the most efficient at producing neutrinos in spite of the lower dissipation rate since very efficient angular momentum transport drains the inner disk much too rapidly.

Previous studies (Di Matteo, Perna & Narayan 2002; Lee, Ramirez-Ruiz & Page 2004, 2005) have shown that at very high accretion rates, greater than approximately one solar mass per second, the neutrino luminosity saturates and the accretion efficiency decreases, inhibiting the driving of winds from the disk (Di Matteo, Perna & Narayan 2002). For the cases computed here, regardless of the actual value of angular momentum considered, the flow never becomes strongly opaque to its own neutrino emission in the sense that the emitted energy is able to escape, thus

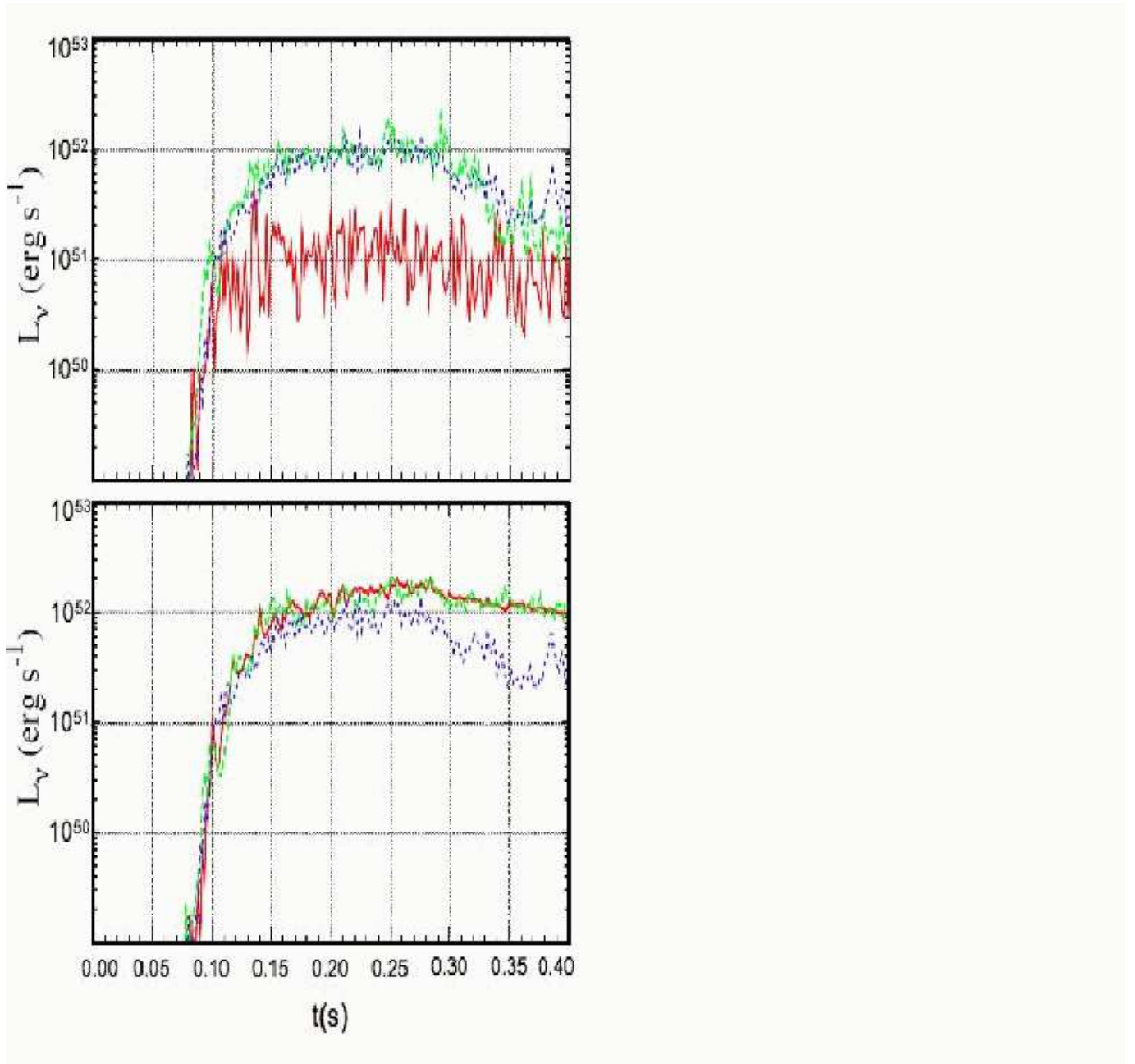


FIG. 11.— Upper panel: Neutrino luminosity  $L_\nu$  for a fixed value of  $\alpha = 0.10$  and different angular momentum values:  $(J_0, \alpha) = (2r_g c, 0.1)$  (red solid line),  $(J_0, \alpha) = (2.5r_g c, 0.1)$  (green dashed line), and  $(J_0, \alpha) = (3r_g c, 0.1)$  (blue dotted line). Lower panel: Neutrino luminosity  $L_\nu$  for a fixed angular momentum  $J_0 = 3.0r_s c$  and varying  $\alpha = 0.00$  (red solid line),  $\alpha = 0.01$  (green dashed line), and  $\alpha = 0.10$  (blue dotted line).

avoiding this limitation. Resolving this issue in more detail requires exploring a wider range of progenitors and longer timescales than those considered here and is beyond the scope of the present paper.

#### 4. DISCUSSION AND CONCLUSIONS

##### 4.1. *Limitations and comparison to other work*

As with all numerical work, the choices made in carrying out the simulations reflect intentions and biases, and the current investigation lacks in several aspects. For example, being a two-dimensional calculation, self-gravity has been considered only in an approximate manner, and stability issues that relate to this or are intrinsically three-dimensional (such as spiral arms) are ignored.

Magnetic fields have not been included and are in all likelihood important in several aspects, two of which deserve special mention. The first is simply that magnetic fields are thought to be at the origin of the magneto rotational

instability (MRI) (Balbus & Hawley 1998) responsible for angular momentum transport and dissipation, which we have considered through the  $\alpha$  parameter. The MRI likely operates in collapsars, although the details of how it does so are likely to be different than what we can infer about it from theory and observation of accretion disks in CVs and X-ray binaries in a more leisurely state of affairs. The second point is related to the importance of magnetic pressure in possible outflows emanating from a disk. Detailed GR MHD calculations (De Villiers, Hawley & Krolik 2005) show that a flow starting from an equilibrium torus develops the MRI and produces an inner dense disk, a funnel wall, and a corona around the central BH. Gas pressure dominates largely in the first, so our hydrodynamical solution to the inner disk is likely to be a realistic approximation, while magnetic pressure is relatively more important in the other two, and being polar structures they are important for the driving of outflows and energy release in the context of GRBs (McKinney & Narayan 2007). For very rapidly rotating BHs, Krolik, Hawley & Hirose (2005) have shown that the magnetic field can actually have a dynamical effect on the mass accretion rate, suppressing it in the inner regions (in their case the Kerr parameter was  $a = 0.998$ ), although a full evaluation of this deserves further study.

GR, approximated in this work simply by use of the Paczyński–Wiita potential, is likely to play a role as well. The location of the horizon and last stable orbit are functions of the rotation of the BH, lying at  $r_H = 2GM/c^2$ ,  $GM/c^2$  and  $r_{\text{ISCO}} = 6GM/c^2$ ,  $3GM/c^2$  for  $a = 0, 1$  respectively, and this is important since most of the energy is released at small radii. For our purposes, however, they are not likely to be crucial since the relevant radii shift appreciably only for very rapidly rotating holes (with  $a$  above 0.7 or so), and the progenitor stars do not easily reach such high values (model 16TI has  $a = 0.44$ ). A secondary aspect of GR is related to the efficiency for  $\nu\bar{\nu}$  annihilation and the corresponding energy release. Some energy is directly lost to the BH because of the strong gravitational field, while focusing increases the annihilation efficiency. Recently Birkel, Aloy & Janka (2007) have carefully computed the energy deposition rates and efficiencies for annihilation in the Kerr metric for various BH spin rates and flow geometries. They find that the power output is affected by approximately up to a factor of 2, depending on whether the disk is geometrically thin or thick (or even for spherical configurations of the neutrinosphere). Thus the general energy scale is affected, but not crucially so.

On the other hand, our effort has been directed here at improving the thermodynamical treatment and that of neutrinos, as well as in considering realistic initial conditions derived from stellar evolution calculations. The choice of inner boundary means that the dense, inner disk producing most of the luminosity is well resolved and treated appropriately. A final point that deserves improvement is clearly the distribution of angular momentum, since having a constant value at all radii is not realistic. We have chosen it for now to gauge the effect of other changes when compared to previous work, and provide a guide in further investigation, which will fully explore situations in which the radial part is a characteristic function of radius (D. Lopez-Camara et al. 2008, in preparation).

With this in mind, we may consider the implications for GRB production and GRB/SN associations following core collapse and prompt BH formation from this set of calculations.

#### 4.2. Global energetics

The fact that we have placed the inner numerical boundary fairly close to the BH (at  $r_{\text{in}} = 20$  km) allows us to directly and more realistically compute the energy release (obviously at the cost of a shorter simulation in time). This is similar to what was done by Lee & Ramirez-Ruiz (2006) and so we can directly compare the two sets of results. The two most important differences between the two studies are in the use of a better equation of state and neutrino treatment here, and in the use of initial models taken from stellar evolution calculations. The neutrino luminosities are higher in the present study, partly because of the more realistic physics employed, but also because of the initial conditions, which directly result in higher accretion rates and densities. Since the cooling rate from captures scales with the density, this fact alone will raise the luminosity. The rates are quite sensitive to the temperature, but the rise in the postshock material is mostly due to the infall kinetic energy per unit mass and is fixed by the potential well of the central BH. It is clear as well, from the results presented for simplified cases in the adiabatic and isothermal limits, and from the computation of the Kelvin–Helmholtz timescale, that correctly accounting for the energy sinks is a crucial ingredient if one wishes to estimate the global energy release and flow properties. Finally, the emergent neutrino spectrum is a function of the angular momentum of the infalling gas, through the selection of the dominant cooling mechanism. This is admittedly a difficult issue to resolve observationally, but may impact upon the energy deposition rate.

The two most important variables that determine the global morphology are the rotation rate, quantified here through the distribution of specific angular momentum, and the strength of angular momentum transport, parameterized through the prescription of Shakura & Sunyaev. It is interesting to note that for high angular momentum (larger than the threshold for disk formation), viscous dissipation is responsible for the production of large-scale flows, namely by producing an outward moving shock after a certain delay (a few tenths of a second). The effect is to perturb the flow into the inner disk and decrease the luminosity. The impact on the flow at large radii remains to be explored in greater detail due to the limitation of our outer boundary.

#### 4.3. Implications for GRB production

The compression for low angular momentum cases releases a large amount of energy, not more than 1 order of magnitude smaller than for the case with a disk, and we believe this to be an important issue: slowly rotating models are in principle capable of releasing an amount of energy that could produce GRBs, although admittedly perhaps only at the faint end of the luminosity distribution. For a 1% efficiency of conversion into pairs through  $\nu\bar{\nu}$  annihilation

at  $L_\nu = 10^{53}$  erg s $^{-1}$ , the models shown here can produce annihilation luminosities of about  $10^{48} - 10^{49}$  erg s $^{-1}$ , depending on the value of  $J_0$ . Performing realistic runs for longer times is a priority, but clearly over long timescales, having slow rotation is not necessarily a handicap regarding the energy release. The simple reason is that, as known for a long time, and first quantified in this scenario by Lee & Ramirez-Ruiz (2006), it is most efficient in terms of energy extraction to have the material release its energy as close as possible to the BH, or equivalently, as deep as possible in the potential well, but not too close so that it is still shocked by the presence of a centrifugal barrier. Magnetic mechanisms may also power fully or partially a potential burst, and we note here only that the internal energies are high enough, as in the most common hypercritical accretion scenarios, to do so if a fraction of this is transferred to a magnetic field (at a level of 10% of equipartition).

The obvious implication in terms of the type of progenitor one can consider for GRBs is that single stars at the threshold for disk formation through centrifugal support are capable of giving a GRB. Having a substantial amount of rotation will obviously guarantee an accretion disk, but perhaps not all cases require such special conditions (as for example, torquing of the pre-SN star by a binary companion). The isotropic equivalent energy of GRB060505 is  $\log[E_{\gamma,\text{iso}}] \simeq 49.5$ , clearly within the range obtainable with the models presented here even at low rotation rates.

#### 4.4. Nucleosynthesis in the outflow and GRB/SN association

Centrifugally supported collapsar disks are expected to produce strong winds (MacFadyen & Woosley 1999), driven quite generically by a combination of viscous, neutrino, and magnetic effects (the first two of which we have explicitly included here). Pruet et al. (2004) in particular, computed the expected nucleosynthesis of  $^{56}\text{Ni}$  in these outflows, using the steady state disk models of Popham, Woosley & Fryer (1999) as an initial condition and considering various mass accretion and dissipation rates. The essential feature of these models is the computation of the change in entropy per baryon,  $s_b/k$  in the outflow, starting from the midplane of the accretion disk and reaching a large distance at which the velocity approaches an asymptotic value  $v_w/c \simeq 0.1 - 0.2$ . From our hydrodynamical determination of the disk structure using an improved equation of state and thermodynamics, we computed the equivalent entropies in the disk and applied the formalism of Pruet et al. (2004) to compute the total change in  $s_b/k$  (assuming the wind reaches similar velocities, unresolved in our simulations spanning 0.5 s). The mass fraction converted to  $^{56}\text{Ni}$ ,  $X_{\text{Ni}}$ , then depends sensitively on  $s_b/k$  and the ratio  $\beta = \dot{M}_o/v_w^3$ , where  $\dot{M}_o$  is the mass outflow rate and  $v_w$  is the terminal wind velocity. Once the outflow is launched we can obtain an estimate of  $\dot{M}_o$  directly from the momentum field in the simulation, and  $v_w/c$  is taken as  $\simeq 0.2$ . We find that for  $J_0 > J_{\text{crit}}$ , and independently of the strength of angular momentum transport, substantial Ni synthesis occurs ( $X(^{56}\text{Ni}) \approx 0.5$ ) in an outflow with  $\dot{M} \approx 0.3 M_\odot \text{ s}^{-1}$ . This would imply a total ejection of  $\simeq M_\odot$  in  $^{56}\text{Ni}$  in a GRB lasting 10 seconds, in the right range to account for the outflows seen, e.g., in SN2003dh. The relatively narrow range in  $J_0$  spanned in our calculations does not allow for a good extrapolation to higher rotation rates, but clearly the amount of mass involved is significant, and would likely grow substantially at higher  $J_0$  where more massive and more radially extended disks are expected (Pruet et al. (2004) estimate several  $M_\odot$  for the massive, centrifugally supported disks taken from Popham, Woosley & Fryer (1999)). A configuration in which no significant outflows occur because the rotation rate is too low ( $J \leq J_{\text{crit}}$ ) would not be expected in this scenario to produce any significant ejection of radioactive elements capable of producing a SN-like signature. It could, as shown here, still release enough energy through neutrinos or magnetic mechanisms to power a classical GRB. The result, if it were to occur at low redshift, could possibly be an event resembling GRB060505.

We thank S.E. Woosley and A. Heger for making their pre-SN models available. This work was supported in part by CONACyT (45845E, WL), PAPIIT-UNAM (IN113007, WL), NASA (Swift NX07AE98G, ER-R) and DOE SciDAC (DE-FC02-01ER41176, ER-R). D.L.-C. acknowledges support through a CONACyT graduate scholarship. W.H.L. thanks the Department of Astronomy and Astrophysics at the University of California, Santa Cruz for hospitality. We thank an anonymous referee for his comments and suggestions in improving the paper.

#### REFERENCES

- Balbus, S. A. & Hawley, J. F. 1998 *Rev. Mod. Phys.*, 70., 1  
 Beloborodov, A. M. 2003, *ApJ*, 588, 931  
 Beloborodov, A. M., & Illarionov, A. F. 2001, *MNRAS*, 323, 167  
 Birkel, R., Aloy, M. A. & Janka, H. T., 2007, *A&A*, 463, 51  
 Blinnikov, S. I., Dunina-Barkovskaya, N. V., & Nadyozhin, D. K. 1996, *ApJ*, 106, 171  
 Bloom, J. S., Kulkarni, S. R., & Djorgovski, S. G. 2002, *ApJ*, 123, 1111  
 Campana, S., et al. 2006, *Nature*, 442, 1008  
 Cantiello, M.; Yoon, S.-C.; Langer, N.; Livio, M. 465, L29  
 Chevalier, R.A. 1989, *ApJ*, 346, 847  
 Della Valle, M., et al. 2003, *A&A*, 406, L33  
 Della Valle, M., et al. 2006a, *ApJ*, 642, L103  
 Della Valle, M., et al. 2006b, *Nature*, 444, 1050  
 Dessart, L., Burrows, A., Livne, E., Ott, C. D. 2008, *ApJ*, 673, L43  
 Detmers, R. G.; Langer, N.; Podsiadlowski, Ph.; Izzard, R. G. 2008 *A&A*, 484, 831  
 Dezalay, J. P., et al. 1996, *ApJ*, 471, L27  
 De Villiers, J.-P., Hawley, J. F. & Krolik, J. H. 2005, *ApJ*, 599, 1238  
 Di Matteo, T., Perna, T., & Narayan, R. 2002, *ApJ*, 579, 706  
 Eichler, D., Livio, M., Piran, T., Schramm, D.N. 1989, *Nature*, 340, 126  
 Fishman, G. J., Meegan, C. A. 1995, *ARA&A*, 33, 415  
 Fynbo, J. P. U., et al. 2006, *Nature*, 444, 1047  
 Fruchter, A. S. et al. 2006, *Nature*, 441, 463  
 Galama, T. J., et al. 1998, *Nature*, 395, 670  
 Gal Yam, A., et al. 2006, *Nature*, 444, 1053  
 Gehrels, N., Cannizzo, J.K., Norris, J.P. 2007, *New J. Phys.*, 9, 37  
 Gehrels, N., et al. 2006, *Nature*, 444, 1044  
 Gorosabel, et al. 2005, *A&A*, 444, 711  
 Heger, A., Woosley, S.E., Spruit, H.C. 2005, *ApJ*, 626, 350

- Heger, A., et al. 2000, *ApJ*, 528, 368  
Houck, J.C., Chevalier, R.A., 1991, *ApJ*, 376, 234  
Itoh, N., et al. 1996, *ApJS*, 102, 411 Itoh et al. (1996)  
Izzard, R.G., Ramirez-Ruiz, E., Tout, C. A. 2004 *MNRAS*, 348, 1215  
Janiuk, A., & Proga, D. 2008, *ApJ*, 675, 519  
Janiuk, A., Yuan, Y., Perna, R., & Di Matteo, T. 2007, *ApJ*, 664, 1011  
Kaneko, Y., et al. 2008, *ApJ*, 654, 385  
Klebesadel, R.W., Strong, I.B., Olsson, R.A. 1973, *ApJ*, 182, L85  
Krolik, J. H., Hawley, J. F. & Hirose, S. 2005, *ApJ*, 622, 1008  
Lattimer, J. M., & Schramm, D. N. 1974, *ApJ*, 192, L145  
Lattimer, J. M., & Schramm, D. N. 1976, *ApJ*, 210, 549  
Langanke, K., & Martínez-Pinedo Lattimer, G. 2001, *At. Data Nucl Data Tables*, 79, 1  
Lee, W. H., & Ramirez-Ruiz, E. 2002, *ApJ*, 577, 893  
Lee, W. H., & Ramirez-Ruiz, E. 2006, *ApJ*, 641, 961  
Lee, W. H., & Ramirez-Ruiz, E. 2007, *New J. Phys.*, 9, 17  
Lee, W. H., Ramirez-Ruiz, E. & Page, D. 2004, *ApJ*, 608, L5  
Lee, W. H., Ramirez-Ruiz, & E., Page, D. 2005, *ApJ*, 632, 421  
MacFadyen, A. I., & Woosley, S. E. 1999, *ApJ*, 524, 262  
McKinney, J. C. & Narayan, R. 2007, *MNRAS*, 375, 513  
Malesani, D., et al. 2004, *ApJ*, 609, L5  
Meegan, C. A., et al. 1992, *Nature*, 355, 143  
Mendoza, S., Tejada, E., & Nagel, E. 2009, *MNRAS*, 393, 579  
Mészáros, P. 2002, *ARA&A*, 40, 137  
Mészáros, P., & Rees, M. J. 1997, *ApJ*, 482, L29  
Metzger, M. R., et al. 1997, *Nature*, 387, 878  
Monaghan, J.J. 1992, *ARA&A*, 30, 543  
Nakar, E., 2007, *Phys. Rep.*, 442, 166  
Narayan, R., Paczyński, B., Piran, T. 1992, *ApJ*, 395, L83  
Narayan, R., Piran, T., & Kumar, P. 2001, *ApJ*, 557, 949  
Paczynski, B. 1986, *ApJ*, 308, L43  
Paczynski, B. 1991, *Acta Astron.*, 41, 257  
Paczynski, B., & Wiita, P. J. 1980, *A&A*, 88, 23  
Piran, T. 2004, *Rev. Mod. Phys*, 76, 1143  
Popham, R., & Narayan, R. 1995, *ApJ*, 442, 337  
Popham, R., Woosley, S. E., & Fryer, C. 1999, *ApJ*, 518, 356  
Prochaska, J. X., et al. 2004, *ApJ*, 611, 200  
Proga, D., & Begelman M. C. 2003, *ApJ*, 582, 69  
Proga, D., MacFadyen, A. I., Armitage, P. J., & Begelman, M. C. 2003, *ApJ*, 599, L5  
Pruet, J., Thompson, T. A., Hoffman, R. D. 2004, *ApJ*, 606, 1006  
Ramirez-Ruiz, E., Granot, J., Kouveliotou, C., Woosley, S.E., Patel, S.K., Mazzali, P.A. 2005, *ApJ*, 625, L91  
Salpeter, E. E. 1964, *ApJ*, 140, 796  
Shakura, N. I., & Sunyaev, R. A. 1973, *A&A*, 24, 337  
Shapiro S. L., & Teukolsky, S. A. 1983, "Black Holes, White Dwarfs, and Neutron Stars: The Physics of Compact Stars (New York: Wiley-Interscience).  
Soderberg, A. M., et al. 2005, *ApJ*, 627, 877  
Sollerman, J., et al. 2005, *New Astronomy*, 11, 103-115  
Sprituit, H.C. 2002, *A&A*, 381, 923  
Stanek, K. Z., et al. 2003, *ApJ*, 591, L17  
Thompson, C. 1994, *MNRAS*, 270, 480  
Usov, V. V. 1992, *Nature*, 357, 472  
van Paradijs, J., Kouveliotou, C., Wijers, R.A.M.J. 2000, *ARA&A*, 38, 379  
Woosley, S. E. 1993, *ApJ*, 405, 273  
Woosley, S.E., Bloom, J.S. 2006, *ARA&A*, 44, 507  
Woosley S. E., & Heger A. 2006, *ApJ*, 637, 914  
Yoon, S.C., Langer, N., 2005, *A&A*, 443, 643  
Zel'Dovich, Y. B. 1964, *Soviet Physics Doklady*, 9, 195